HHS Public Access

Author manuscript

Nat Struct Mol Biol. Author manuscript; available in PMC 2011 September 01.

Published in final edited form as:

Nat Struct Mol Biol. 2011 March ; 18(3): 364–371. doi:10.1038/nsmb.1990.

Defining an allosteric circuit in the cysteine protease domain of *Clostridium difficile* toxins

Aimee Shen[1,*], **Patrick J. Lupardus**[2,3,7], **Aaron W. Puri**[4], **Victoria E. Albrow**[1,8], **Malte M. Gersch**[5], **K. Christopher Garcia**[2,3], and **Matthew Bogyo**[1,6,*]

[1]Department of Pathology, Stanford School of Medicine, Stanford, California, USA

[2]Department of Molecular and Cellular Physiology Stanford School of Medicine, Stanford, California, USA

[3]Howard Hughes Institute, USA, Stanford School of Medicine, Stanford, California, USA

[4]Department of Chemical and Systems Biology, Stanford School of Medicine, Stanford, California, USA

[5]Department of Chemistry and Biochemistry, Ludwig Maximilians University (LMU) Munich, Germany

[6]Department of Microbiology and Immunology, Stanford School of Medicine, Stanford, California, USA

Abstract

An internal cysteine protease domain (CPD) autoproteolytically regulates *Clostridium difficile* glucosylating toxins by releasing a cytotoxic effector domain into target cells. CPD activity is itself allosterically regulated by the eukaryotic-specific molecule inositol hexakisphosphate ($InsP_6$). Although allostery controls the function of most proteins, the molecular details underlying this regulatory mechanism are often difficult to characterize. Here we use chemical probes to show that apo-CPD is in dynamic equilibrium between active and inactive states. $InsP_6$ dramatically shifts this equilibrium towards an active conformer that is further restrained upon binding a suicide substrate. Structural analyses combined with systematic mutational and disulfide bond engineering studies reveal that residues within a β-hairpin region functionally couple the $InsP_6$ binding site to the active site. Collectively, our results identify an allosteric circuit that allows bacterial virulence factors to sense and respond to the eukaryotic environment.

Allostery is central to the regulation of many cellular processes. This ubiquitous mechanism refers to the control of protein behavior at a distance, with a change at one site (the allosteric

[*]To whom correspondence should be addressed: Matthew Bogyo mbogyo@stanford.edu Tel # 650-725-4132 or Aimee Shen ashen2@stanford.edu.

[7]Current Address: Genentech, Inc, South San Francisco, California, USA

[8]Current Address: Pfizer, Inc, Sandwich, UK.

Accession codes. Coordinates and structure factors have been deposited in the Protein Data Bank (www.rcsb.org) under accession number 3PEE.

site) affecting the function at a second. The functional coupling between these two sites is often mediated through structural rearrangements1. Well-characterized examples include the cooperative binding of oxygen to hemoglobin, whereby ligand binding at the allosteric site alters protein function through changes in quaternary structure (for review see2–4). Although conformational changes induced by allosteric effectors can frequently be detected, understanding *how* these structural alterations translate into changes in function is typically more challenging. This is because defining an allosteric signaling pathway requires the identification of specific amino acids that couple changes in structure or dynamics to changes in function.

The regulation of the *Clostridium difficile* glucosylating toxin cysteine protease domain (CPD) by the small molecule inositol hexakisphosphate ($InsP_6$) is an ideal system for studying allosteric signaling pathways5–8. *C. difficile* CPDs belong to a conserved family of autocatalytic proteases within bacterial toxins that are allosterically activated by $InsP_6$, a metabolite found abundantly in the eukaryotic cytosol6,9. These clan CD protease members cleave exclusively on the C-terminal side of a leucine residue to liberate toxin effectors from receptor binding domains and other effectors7,10–13. $InsP_6$ activates bacterial CPDs by binding to a basic cleft that is distinct from the active site. This binding event induces conformational changes that are presumably linked to protease activation11,14,15. More specifically, $InsP_6$ has been proposed to induce rearrangement of a β-hairpin structure to permit formation of the substrate binding pocket and alignment of the catalytic residues11,14,15.

C. difficile CPDs function to autocatalytically cleave the glucosylating toxins TcdA and TcdB at a single site to liberate a cytotoxic effector domain into target cells12,16. This event occurs at the later stages of a multi-step intoxication process17,18. Glucosylating toxins first enter cells using receptor-mediated endocytosis; during acidification of the endosome, they undergo a conformational change that mediates toxin translocation across the endosomal membrane. Exposure of the CPD to $InsP_6$ in target cells activates the protease, resulting in autocatalytic cleavage. This autoprocessing event releases the glucosyltransferase domain from the endosome into the cytosol and presumably enhances glucosyltransferase binding to its Rho GTPase substrates at the plasma membrane19. Glucosylation of Rho GTPases inhibits their function, leading to cell rounding and ultimately cell death17.

Notably, the glucosylating toxins of *C. difficile* are the primary virulence factors of this important and emergent nosocomial pathogen20,21, and TcdB alone is sufficient to cause disease22. Because *C. difficile* is naturally antibiotic resistant, there is great interest in developing therapeutics that target glucosylating toxin function20,21,23. A more thorough understanding of CPD-mediated regulation of these toxins would likely facilitate the design of such therapeutics, since CPD activity is necessary for optimal toxin function7,10. Understanding how the *eukaryotic-specific* small molecule $InsP_6$ activates the CPD would further provide mechanistic insight into how allostery integrates environmental signals to regulate protein function.

In this study, we examined the mechanism underlying the allosteric activation of *C. difficile* TcdB CPDs by $InsP_6$. Using a combination of structural analyses and an activity-based

probe specific for TcdB CPD, we show that, even in the absence of $InsP_6$, TcdB CPD transiently samples the activated conformation. $InsP_6$ binding shifts the conformational equilibrium of the enzyme to an active conformer that is further stabilized by reaction with a suicide substrate. Using mutational studies, we demonstrate that adoption of this activated conformation depends upon an interconnected network of residues that functionally couple $InsP_6$ binding to protease activation. These results therefore provide detailed mechanistic insight into a tightly controlled allosteric regulatory system used by a large family of bacterial pathogens. This information may facilitate the discovery of allosteric circuits in other systems and is likely to aid in the development of therapeutic agents that disrupt such networks.

Results

Measuring TcdB activation with an activity-based probe

In order to dynamically monitor the $InsP_6$-induced activation of *C. difficile* TcdB CPD, we sought to develop a reliable assay. Although autoprocessing can be used as a measure of $InsP_6$-induced activation of TcdB CPD (Supplementary Fig. 1), this assay lacks the sensitivity needed to accurately measure the kinetics of this process. Fluorogenic substrate assays for the CPD also lack sensitivity because high substrate concentrations are needed to generate detectable activity14. In contrast, activity-based probe (ABP) labeling can be used to sensitively detect $InsP_6$-induced CPD activation24 (Fig. 1a). ABPs are small molecules that exclusively label active enzyme25,26. ABPs contain an electrophilic group that can only react with the active site nucleophile of an enzyme when the protein has assumed a catalytically competent conformation. We previously developed an ABP, AWP19, that specifically labels the CPD of full-length TcdB24. This probe consists of (i) an acyloxymethyl ketone (AOMK) reactive group that covalently modifies the catalytic Cys of clan CD proteases27–29, (ii) a Ser-Leu peptide sequence that directs inhibitor binding to the CPD24, and (iii) a Cy5 fluorophore tag that permits detection of the labeled enzyme. The Ser-Leu specificity element of AWP19 was identified by screening a small positional scanning library of inhibitors against TcdB CPD24.

Titration of $InsP_6$ against TcdB CPD in the presence of excess AWP19 resulted in a dose-dependent labeling of the protease in a manner dependent on the catalytic Cys (Fig. 1b). This analysis yielded an activation constant (EC_{50}) for TcdB CPD of 0.17 ± 0.06 μM (Fig. 1c), the concentration of $InsP_6$ at which probe labeling is half maximal. Notably, this value is identical to the EC_{50} determined using the standard autocleavage assay (Supplementary Fig. 1), validating AWP19 as a tool for measuring CPD activation.

Because AWP19 covalently labels the target only when the active site forms, it can be used to monitor the activation state of the CPD. We exploited this property to determine whether TcdB CPD could achieve an activated conformation independent of $InsP_6$. Probe labeling with AWP19 indicated that approximately 10% of apo-CPD could be labeled in the absence of $InsP_6$, whereas the catalytic Cys mutant was not labeled at all (Fig. 1b). Furthermore, incubation of apo-CPD with probe for an extended period of time resulted in a time-dependent increase in labeling, with ~70% of the apo-enzyme being labeled after 16 hr (Fig. 2a). Likewise, pre-incubation of apo-CPD with an unlabeled CPD-specific inhibitor (Ac-

GSL-AOMK24) was sufficient to block probe labeling of the CPD in a time-dependent manner (Fig. 2b), with ~70% of apo-CPD modified by the inhibitor after 16 hr treatment. The observed probe labeling of apo-CPD was not due to contamination with $InsP_6$ during CPD purification from *E. coli* grown in $InsP_6$-containing LB media, since apo-labeling was also observed when the CPD was purified from *E. coli* grown in minimal media (data not shown). These results demonstrate that apo-TcdB CPD can transiently sample the activated conformation.

We next used the probe to measure the effect of $InsP_6$ binding on activation of the CPD. Whereas TcdB CPD labeling in the absence of $InsP_6$ occurred very slowly (0.91 AU min^{-1}, Fig. 2c **inset**), $InsP_6$ dramatically increased the rate of labeling in a dose-dependent manner (142 AU min^{-1} at 1 μM $InsP_6$, Fig. 2). Furthermore, we observed that ~20% of the $TcdB_{1–804}$ autocleavage substrate undergoes CPD-dependent autoprocessing when produced in the $InsP_6$-free environment of *E. coli* (Supplementary Fig. 2). These observations indicate that the TcdB CPD containing an N-terminal extension can also adopt the "ON"-state during expression in *E. coli*. Interestingly, this transient sampling of the "ON"-state by the apo-enzyme was specific to TcdB CPD, since expression of the related *V. cholerae* MARTX CPD in *E. coli* did not result in autoprocessing,14,30,31 and *V. cholerae* CPD did not react with AWP19 in the absence of $InsP_6$(Fig. 2, Supplementary Fig. 3). Together these results support the conclusion that apo-TcdB CPD can adopt an activated conformer in the absence of $InsP_6$ and that $InsP_6$ binding directly enhances the reactivity of the catalytic Cys by shifting the conformational equilibria of TcdB CPD to an activated form.

Small molecule binding and CPD conformational mobility

In order for the AWP19 probe to label TcdB CPD, the protease must productively bind the peptide as it would a protein substrate13,24. In related clan CD proteases, this inhibitor binding event has been shown to "lock" these enzymes in an active conformation32,33. We questioned whether binding of a covalent inhibitor in the CPD active site might similarly induce retention of the enzyme in an active confirmation. Therefore we examined the effect of inhibitor modification on the conformational dynamics of TcdB CPD. To determine if the peptide backbone of the probe was required to constrain the CPD in the active form, we compared the effect of modifying TcdB CPD with the AOMK probe relative to the general alkylating agent N-ethylmaleimide (NEM). We used limited proteolysis as a read-out for conformational mobility, since this assay has previously been used to demonstrate that $InsP_6$ stabilizes a protease-resistant conformation of *C. difficile* CPDs5,15 (Fig. 3a, untreated). Covalent modification of apo-TcdB CPD by either inhibitor did not affect the limited proteolysis profile relative to untreated enzyme (Fig. 3a, (–) panel), indicating that covalent modification alone is not sufficient to protect the enzyme from protease degradation. However, when $InsP_6$ was added to these variants, AOMK treated but not NEM-modified CPD showed increased protection from protease degradation (Fig. 3a**, (+) panel**). Covalent modification of TcdB CPD by either NEM or AOMK inhibitor blocked AWP19 labeling of these variants, indicating that the catalytic Cys of both variants were modified to similar extents (Supplementary Fig. 4). These results suggest that inhibitor modification in the context of substrate recognition is necessary to shift the equilibrium to a more stable conformer upon $InsP_6$ addition.

Since the TcdB CPD used in these analyses had been covalently modified in its *apo*-form, we tested the effect of covalently modifying TcdB CPD in the *presence* of $InsP_6$. Therefore we covalently modified TcdB CPD with either peptide AOMK or NEM in the presence of $InsP_6$, re-purified the enzyme after these treatments, and subjected the TcdB CPD variants to complete trypsin digestion. As expected, only AOMK-modification of the CPD, and not NEM, modification markedly stabilized the enzyme (Fig. 3b). Notably, $InsP_6$ treatment increased the stability of the CPD even after re-purification of the enzyme, suggesting that $InsP_6$ remains associated with TcdB CPD during this procedure (Fig. 3b). These findings indicate that, while $InsP_6$ binding to TcdB CPD can restrict its conformational dynamics, substrate binding by the protease further constrains the protease in the active form.

Another measure of TcdB CPD conformational mobility is its ability to release $InsP_6$ after the re-purification procedure. We therefore created an assay that measures the activation of $MARTX_{Vc}$ CPD as a result of transfer of $InsP_6$ from TcdB CPD. Whereas no activation of the $MARTX_{Vc}$ CPD was observed upon addition of apo-TcdB CPD, addition of either $InsP_6$-treated TcdB CPD or NEM-bound, $InsP_6$-treated TcdB CPD markedly increased its activity (Fig. 3c). In contrast, addition of $InsP_6$-treated TcdB CPD covalently modified by the AOMK peptide inhibitor resulted in only a minimal increase in $MARTX_{Vc}$ CPD activity. Complete trypsin digestion of all $InsP_6$-treated TcdB CPD variants, including NEM-bound and AOMK-bound, confirmed that similar levels of $InsP_6$ were bound to each (Fig. 3c). Together, these results suggest that substrate recognition by an $InsP_6$-bound TcdB CPD restrains its conformational mobility such that it cannot release $InsP_6$ without complete degradation of the protein. Thus, substrate recognition by TcdB CPD, in the context of binding to $InsP_6$, would appear to "rigidify" the enzyme.

Effect of substrate binding on TcdB CPD structure

To gain insight into the effect of substrate binding on TcdB CPD conformation in the presence of $InsP_6$, we solved the crystal structure $InsP_6$-bound TcdB CPD (Fig. 4a) and compared it to the AOMK modified, $InsP_6$-bound TcdB CPD24. Not surprisingly, the structure of TcdB CPD is highly similar to that of the recently reported structure of its close homolog (56% identity) TcdA CPD15 (rmsd of 1.3Å). Most of the sequence differences between the two CPDs are found outside of regions involved in $InsP_6$ binding and catalytic activity. The active site residues are completely conserved (Fig. 4b), and residues in the $InsP_6$ binding site are also conserved with the minor exception of two conservative basic substitutions (Lys577→Arg575, Lys754→Arg752) (Fig. 4c). Core residues essential to the structure of the β-flap are also well conserved, including the π-cation interaction of Arg745 and Trp761 as well as Leu755, Glu753, and Asn747 (discussed below). While moderately divergent at the sequence level, the structural elements necessary for $InsP_6$ binding and P1 leucine selectivity are tightly conserved in the TcdA and TcdB CPDs.

Comparison of the $InsP_6$-bound TcdB CPD structure with that of $InsP_6$-bound TcdB covalently modified by an Ac-GSL-AOMK peptide in the active site (PDB ID 35A824) shows that the two structures are essentially superimposable (rsmd of 0.6 Å, Supplementary Fig. 5). This observation implies that the active site forms upon $InsP_6$ binding and furthermore that substrate binding does not make an induced fit. This is consistent with the

previous observation that inhibitor binding does not alter the structure of $InsP_6$-bound *V. cholerae* MARTX CPD13. These results suggest that the allosteric activation mechanism induced by $InsP_6$ binding organizes the active site so that it can directly bind substrate.

Tryptophan fluorescence identifies an allosteric circuit

As in previous structures of bacterial CPDs, $InsP_6$ binds to a positively charged cleft that is distal from the active site, and an antiparallel β-hairpin structure (termed the β-flap) appears to bridge the $InsP_6$ and substrate binding pockets11,13–15. This β-flap structure has been proposed to form upon $InsP_6$ binding to the protease6,8, since residues on one side of the β-flap interact with $InsP_6$, while residues on the other side form the substrate binding pocket (Fig. 4). In $MARTX_{Vc}$ CPD, residues within this region have been shown to respond to $InsP_6$ binding11. Nevertheless, in the absence of an apo-structure, the precise conformational changes that occur upon $InsP_6$ binding remain unknown.

To test whether $InsP_6$-induced conformational rearrangements in the β-flap region could be detected in TcdB CPD, we developed an assay that monitors the mobility of a conserved β-flap tryptophan found in all bacterial CPDs.6,8 This β-flap Trp helps stabilize the substrate binding pocket of bacterial CPDs and affects the responsiveness of the enzyme to $InsP_6$11,14,15 Since the intrinsic fluorescence of Trp is strongly affected by its immediate environment34, we assessed whether $InsP_6$ binding induces changes in the intrinsic fluorescence of β-flap Trp761. Conveniently, Trp761 is the sole Trp in TcdB CPD; thus, all changes in tryptophan fluorescence emission can be attributed to changes in the local environment around this residue. Addition of $InsP_6$ to TcdB CPD resulted in a dose-dependent increase in Trp fluorescence and concomitant decrease in the maximum wavelength of emission (Fig. 5a), consistent with $InsP_6$ binding to the CPD causing Trp761 to enter a more hydrophobic environment34. Thus, Trp fluorescence can be used to sensitively probe structural changes induced by $InsP_6$ in the β-flap region.

In the $InsP_6$-bound structures of TcdA15 and TcdB CPD (Fig. 4), Trp761 appears to be stabilized by a network of interactions that extends from the β-flap down to the $InsP_6$ binding site. Trp761 forms a π-cation interaction with Arg745, while Arg745 is itself stabilized by an electrostatic interaction with Glu753. This latter residue also forms a hydrogen bond with Asn747 which, in turn, hydrogen bonds with the main chain amide of the $InsP_6$-interacting residue, Arg751 (Fig. 6). To determine the functional importance of these interactions on the $InsP_6$-induced movement of Trp761, we examined the effect of mutating β-flap region residues on Trp fluorescence and CPD activity. Conservative mutation of Arg745 severely decreased Trp fluorescence but only slightly affected CPD activity (reduced by a factor of 3), while a stronger mutation (R745Q) completely abrogated Trp fluorescence and diminished CPD function by a factor of 25 (Fig. 5b and c). Disruption of the salt bridge between Arg745 and Glu753 by mutating Glu753 to glutamine resulted in slight decreases in Trp fluorescence shift and CPD activity (Fig. 5b and c), while a more severe mutation to asparagine abrogated the Trp fluorescence change altogether and reduced protease function by a factor of 20. Mutation of Asn747 to alanine similarly reduced the Trp fluorescence shift and decreased CPD activity by a factor of 24. Taken together, the results demonstrate that $InsP_6$-induced changes in Trp fluorescence depend on a network of

interactions between β-flap residues and that changes in Trp fluorescence directly correlate with levels of protease activity.

Similar effects on Trp fluorescence and protease activity were observed upon mutation of $InsP_6$ interacting residues. Disruption of the electrostatic interactions between these residues and $InsP_6$ both decreased Trp fluorescence and protease function (Fig. 5b and d), even though Trp761 is far removed from these $InsP_6$ binding residues. Our finding that Trp fluorescence shifts become saturated even at high $InsP_6$ concentrations suggests that the range of $InsP_6$-induced movement of Trp761 is diminished in the $InsP_6$ binding site mutants relative to wild type. Thus, $InsP_6$-induced movement of Trp761 appears to depend on a network of interactions extending from the $InsP_6$ binding site through the β-flap region.

One possible mechanism for allosteric signaling to the active site involves a network of interactions that have a specific spatial and temporal order2. To explore this possibility, we disrupted the interconnectedness of this network by performing a salt-bridge swap. Residues in the Arg745–Glu753 salt bridge were exchanged to form the R745E E753R double mutant. Although this mutant retains the critical β-flap salt-bridge, it loses the π-cation interaction between Arg745 and Trp761 and the hydrogen bond between Asn747 and Glu753. Accordingly, the activity of the double mutant was decreased by a factor of 23 relative to wildtype TcdB CPD (Fig. 4c). Collectively, these results identify a conduit of interconnected residues that communicate $InsP_6$ binding to the active site.

Disulfide bond engineering the β-flap region

If in fact $InsP_6$ binding directly induces formation of the β-flap, engineering a stabilization of this structure should improve the responsiveness of the CPD to $InsP_6$. To this end, we introduced disulfide bonds designed to stabilize the β-flap structure and examined their effect on protease activity in response to $InsP_6$ (Fig. 6). This approach was possible due to the fact that wildtype CPD does not contain disulfide bridges. Remarkably, introduction of a disulfide bond between helix α4 and strand G_3 of the β-flap (I762C E766C) produced a mutant that was more responsive to $InsP_6$ than wild type (Fig. 6). Reduction of this disulfide bond restored wildtype levels of activity to I762C E766C. A similar redox-responsive effect was observed when a disulfide bond was engineered in the upper β-flap region (L755C W761C; Fig. 6). Furthermore, the L755C–W761C disulfide bond partially complemented the intrinsic defect of the W761C mutant (Fig 6), indicating that stabilization of this region can partially overcome the loss of the Arg745–Trp761 interaction. However, disulfide mutants in the lower portion of the β-flap region had the opposite effect on protease activity (Fig. 6). Replacement of the Arg745–Glu753 salt-bridge with a disulfide bond decreased CPD activity by a factor of ~80 relative to wildtype, whereas reduction of the disulfide bond restored activity close to wildtype levels (Fig. 6). Formation of a disulfide bond across the $InsP_6$ binding site (R751C E765C) also severely hampered CPD function, while addition of reductant largely reversed this defect (Fig. 6). These studies suggest that restraining the mobility of the upper β-flap region enhances the responsiveness of the protease to $InsP_6$, whereas restraining the mobility in the lower portion strongly diminishes its responsiveness to $InsP_6$.

Discussion

Communication between functional sites, or allostery, is central to the regulation of many proteins. In most cases, however, the pathways through which the signal travels are poorly characterized2–4. Here we show that activation of a *C. difficile* cysteine protease domain by its allosteric ligand $InsP_6$ depends upon formation of an orchestrated series of interactions within the β-flap. Our results suggest that the β-flap structure functionally and mechanically couples $InsP_6$ binding to protease activation. Furthermore, our data indicate that, while $InsP_6$ binding rapidly accelerates the formation of this activated conformation, the apo-enzyme can transiently, but detectably, sample the activated conformer.

Using systematic mutational and structural analyses, we identified a conserved set of interconnected residues in the β-flap region that directly communicate the $InsP_6$ signal to the active site. In addition to the $InsP_6$ interacting residues, which are necessary to sense the $InsP_6$ signal (Fig. 4c), this contiguous network involves hydrogen bonding between the $InsP_6$ interacting residue Arg751 and β-flap residues Asn747 and Glu753; a salt-bridge between Glu753 and Arg745; and a π-cation interaction between Arg745 and Trp761. Disrupting the interconnectivity of these interactions reduces protease function, as evidenced by the defect caused by reversing the orientation of the Arg745–Glu753 salt-bridge (Fig. 4c). The allosteric conduit appears to terminate at W761, since mutation of Leu755, a residue within van der Waals bond distance, had essentially no effect on CPD activity (Fig. 6).

These mutational analyses have identified 12 out of 253 CPD residues that participate in $InsP_6$ signaling (Fig. 4c). While additional residues may be involved, perhaps in the substrate binding region, our data are consistent with the view that a small subset of conserved, physically connected residues propagate allosteric signals between distinct functional sites, as was recently shown for caspase−135 and FecA36. Our finding that ~5% of CPD residues participate in this long-range communication is also consistent with other bioinformatic analyses aimed at identifying allosteric circuits in other proteins using co-evolution37.

The tryptophan fluorescence assays indicate that $InsP_6$ signal transduction through this interconnected network of residues results in movement of the conserved β-flap residue W761 into a less solvent exposed environment (Fig. 5). When coupled to activity assays, these biophysical analyses reveal that $InsP_6$-induced structural changes correlate with enzyme activation (Fig. 4c). The disulfide trapping studies further demonstrate that exogenous stabilization of the upper β-flap structure increases the responsiveness of the CPD to $InsP_6$ in a redox-sensistive manner (Fig. 6). Collectively, our results support a model in which the active conformation of TcdB CPD is stabilized by β-flap formation. More broadly, these types of analyses provide a framework for determining how structural alterations in an allosteric circuit couple to changes in protein function.

The emerging view of allostery proposes that allosteric effectors cause a redistribution in the relative populations of protein conformers rather than formation of a *de novo* conformer2–4. Thus, allosteric effectors perturb a *pre-existing* conformational equilibrium2,38. The

activity-based probe labeling experiments provide direct evidence in support of this theory. Because the probe is covalent and activity dependent, we were able to sensitively detect the transient adoption of an active conformer by the apo-enzyme over time (Fig. 2). Our results indicate that probe labeling can be used to dynamically measure protein activation and to detect minor levels of conformers in a given population. We anticipate that activity-based probes25 will be useful tools for biochemically dissecting allosteric mechanisms of regulation for a number of enzyme classes.

The adoption of the activated conformer of the CPD upon $InsP_6$ binding directly correlated with a reduction in its conformational mobility5 (Fig. 3). Furthermore, substrate recognition of a peptide AOMK inhibitor in the presence of $InsP_6$ more severely restrained the conformational dynamics of the CPD. Inhibitor binding and covalent modification of the $InsP_6$-bound TcdB CPD resulted in a protein that was highly resistant to trypsin digestion and did not release its associated $InsP_6$ in the transfer assay (Fig. 3). Notably, a similar stabilization of the CPD was not observed when the active cysteine was modified with the general alkylating agent NEM. Thus, recognition of an optimal peptide substrate, rather than simple covalent inhibition alone, appears to be the primary factor in restraining CPD dynamics in the presence of $InsP_6$ (Fig. 3). We propose that, similar to the caspases33, binding of the critical leucine acts as a “key” that “locks” the enzyme in a catalytically competent conformation. In contrast with the caspases, however, substrate binding does not induce conformational changes in TcdB CPD13,33,39. Rather, $InsP_6$ binding appears to be the driving force behind the structural rearrangements that lead to protease activation, while substrate binding holds the activated conformer in place.

The observation that TcdB CPD remains conformationally flexible in the presence of $InsP_6$ appears critical to its function as a protease. When the lower β-flap region was constrained by disulfide bond formation, protease activity was strongly diminished; in contrast, reduction of the disulfide bonds restored activity to levels similar to wild type (Fig. 6). This latter observation indicates that, even though the double Cys mutations disrupted the allosteric circuit, physically linking Cys residues together was primarily responsible for severely reducing protease function. Interestingly, although the disulfide bond mutants constructed in this study were originally designed to increase the responsiveness of the CPD to $InsP_6$, the majority of engineered disulfide linkages decreased TcdB CPD activity. Only the mutants whose disulfide bonds were engineered proximal to the β-flap (but outside the allosteric conduit defined by this study) resulted in greater responsiveness to $InsP_6$ (Fig. 6). For example, the I762C E766C mutant was predicted to stabilize the interaction between helix α4 and strand G_3 of the β-flap, which in TcdA is linked by a salt bridge15. Covalent linkage of these residues, which are dispensable for protease activity, increased the sensitivity of TcdB CPD to $InsP_6$. It is tempting to speculate that stabilizing the interaction between helix α4 and strand G_3 promotes formation of the β-flap in the presence of $InsP_6$. Future structural analyses of the I762C E766C should allow this hypothesis to be tested.

A similar increase in $InsP_6$ responsiveness was observed upon formation of a disulfide bond between W761C and the neighboring L755C residue relative to the reduced form. In contrast, covalent linkage of W761C to R745C effectively ablated enzyme activity (Fig. 6). Given that Leu755 does not participate in the allosteric conduit (Fig. 5b), but Arg745 is a

key constituent, these results suggest that restraining protein dynamics within the allosteric circuit may impede signal propagation. Although we cannot discount the possibility that the engineered disulfide bonds alter the overall conformation of the β-flap in addition to "rigidifying" this region, this interpretation is consistent with the theory that conformational mobility underlies both allostery and catalysis3,40–42.

Based on these observations, restraining the conformational dynamics of TcdB CPD would appear to be an effective strategy for preventing the activation of *C. difficile* glucosylating toxin function by the CPD43. Inhibitors that prevent the allosteric transition44 or that shift the conformational equilibrium to an inactive conformer45,46 could be more effective and suitable for therapeutic applications than peptidic compounds that target the active site. A clearer understanding of the activation mechanism might also facilitate the identification of cell-impermeable compounds that prematurely activate the protease and thus prevent the cytotoxic activity domain from entering cells. Such approaches will require studies of CPD dynamics in the context of full-length toxin before and after intoxication, since the holotoxin undergoes dramatic structural alterations during translocation47,48. Indeed, a major challenge in understanding the allosteric mechanism that governs the autoproteolytic regulation of *C. difficile* toxin function will be defining how the conformational dynamics of the full-length toxin affects CPD dynamics and function. These studies may further inform our understanding of how $InsP_6$ modulates protein behavior in a more general sense, since this small molecule directly binds to unrelated bacterial effector proteins49 and eukaryotic enzymes involved in diverse processes50–52.

Methods

Bacterial growth conditions and strain construction

Bacterial strains were grown at 37°C in Luria-Bertrani (LB) broth. Antibiotics were used at 100 μg mL^{-1} carbenicillin for pET22b and 30 μg mL^{-1} kanamycin for pET28a vectors in *E. coli*. For details on strain construction, see the Supplementary Methods.

TcdB CPD AWP19 probe labeling assay

TcdB CPD (544–797 aa) was diluted into CPD buffer [60 mM NaCl, 20 mM Tris pH 7.5, 250 mM sucrose] to a final concentration of 1 μM. AWP19 was added to a final concentration of 10 μM (1:100 dilution of a DMSO stock) and then 50 μL aliquots were plated in a 96 well plate. $InsP_6$ (Calbiochem) was added (1:100 dilution from stock in water) to the indicated concentrations in triplicate. AWP19 labeling was allowed to proceed for 1 hr at 37°C after which 30 μL of the reaction was transferred into 10 μL 4 × final sample buffer (FSB) in a second 96 well plate. The reaction was boiled for 3 min at 95°C and then 10 μL was resolved by SDS-PAGE (14% gel). The gel was scanned using a Typhoon imager and then Coomassie stained to ensure equal loading. For the redox sensitivity assays, the AWP19 probe labeling assay was performed as described except that the mastermix was divided into two, and DTT was added to a final concentration of 1 mM.

EC_{50} determination

Labeling reactions were quantified in triplicate using the program ImageJ (imagej.nih.gov/ij, National Institutes of Health). The absolute value for each $InsP_6$ concentration was averaged and then corrected by subtracting the average value at 0 μM $InsP_6$. The corrected values were plotted against $InsP_6$ concentration, and the EC_{50} (the concentration of ligand that produced half-maximal labeling) was determined using the Michaelis-Menten function on KaleidaGraph.

Protein purification

For details see Supplementary Methods.

Kinetics of AWP19 labeling

For details see Supplementary Methods.

Limited Chymotrypsin Proteolysis

TcdB CPD was diluted into 1.0 mL CPD buffer to a final concentration of 100 μM. The mastermix was divided into 3 tubes of 300 μL. Ac-GSL-AOMK was added to one tube to give a final concentration of 200 μM (20 mM stock in DMSO), while NEM was added to a second tube to give a final concentration of 200 μM (50 mM stock in DMSO). The third tube was left untreated. The samples were incubated for 16 hr at room temperature after which they were diluted with 900 μL of low imidazole lysis buffer. Fifty microlitres of Ni-NTA beads were added and incubated with nutation for 1 hr at room temperature; immobilized His_6-tagged TcdB CPD was washed times and then eluted with two times with 100 μL high imidazole buffer. The TcdB CPD variants were then diluted to 18 μM in 10 mM Tris pH 7.5 buffer in a total volume of 300 μL. The mixture was split into two, and 1.75 μL of 10 mM $InsP_6$ was added to one tube for a final concentration of 100 μM. Twenty-four microlitres of the mastermix was aliquoted into a 96 well plate and then chymotrypsin was added to the indicated concentration (1:25 dilution). Limited proteolysis was allowed to proceed for twelve minutes after which 7.5 μL of 4× FSB was added to the reactions. The samples were boiled for 3 min at 95°C and then 10 μL was resolved on a 14% SDS-PAGE gel and visualized by Coomassie staining.

Complete Trypsin digestion

For details see Supplementary Methods.

$InsP_6$ transfer assay

For details see Supplementary Methods.

Crystallization and data collection

For TcdB CPD bound to $InsP_6$, initial crystal hits were observed in 0.1 M Tris HCl pH 8.0 and 30% (w/v) PEG2000 MME as the precipitant. Ultimately, diffraction quality crystals were grown using the sitting drop vapor-diffusion method by mixing 0.5 uL of protein with an equal volume of mother liquor and allowing the crystals to grow for 45 to 60 days. Crystals were cryoprotected in 45% (w/v) PEG2000 MME, and data was collected under

cryo-cooled conditions at 100 K at the Advanced Light Source beamline 8.2.1 (Berkeley, CA). Diffraction data were processed using MOSFLM53 and SCALA54 from the CCP4 suite, and data processing statistics are listed in Table 1. Electron density of the structure is shown in Supplementary Fig. 6.

Structure determination and refinement

Initial phases were obtained by molecular replacement with PHASER55 using the structure of the inhibitor-TcdB complex (PDBID 35A8)24 as a search model. The structure then underwent rounds of restrained refinement with PHENIX56 followed by model adjustment with COOT57, resulting in final R/Rfree values of 19.1 and 24.0%, respectively. Ramachandran analysis of structure geometry with Molprobity indicates 98.1% of residues reside in the most favourable regions, with none in disallowed regions58. Refinement statistics are listed in Table 1. Structural figures were prepared with Pymol59 using chain A in all instances. The final model contains two copies of the TcdB CPD in the asymmetric unit, each bound to one molecule of $InsP_6$ and a single calcium ion bridging the crystal interface between the two CPD molecules in the ASU.

Intrinsic tryptophan fluorescence assay

TcdB CPD variants were diluted to 20 μM in 4.3 mL phosphate buffered saline (PBS) and divided into 600 μL aliquots. $InsP_6$ was added to the indicated concentration (100-fold dilution) and then 190 μL aliquots were added in triplicate to a 96 well clear bottom black plate. The samples were excited at 295 nm, and the emission spectrum was measured at 1 nm increments from 325 nm to 375 nm. $InsP_6$ was also added to PBS as the buffer control. The A280 of the plate was measured, and the average A280 for each prep was determined. The fluorescence values at each wavelength were averaged and the PBS background was subtracted. The resulting relative fluorescence unit (RFUs) was then divided by the average A280 value.

Supplementary Material

Refer to Web version on PubMed Central for supplementary material.

ACKNOWLEDGEMENTS

We would like to thank Jim Wells for helpful suggestions in the preparation of this manuscript. A.S. is supported by an NIH National Institutes of General Medical Sciences K99GM092934. P.J.L. is a Damon Runyon Fellow, supported by the Damon Runyon Cancer Research Foundation. A.W.P. is supported by an NSF Graduate Research Fellowship. K.C.G. is supported by the Keck Foundation and the Howard Hughes Medical Institute. M.B. is supported by the Burroughs Wellcome Foundation and NIH grants R01EB005011 and R01AI078947.

References

1. Changeux JP, Edelstein SJ. Allosteric mechanisms of signal transduction. Science. 2005; 308:1424–8. [PubMed: 15933191]
2. del Sol A, Tsai CJ, Ma B, Nussinov R. The origin of allosteric functional modulation: multiple pre-existing pathways. Structure. 2009; 17:1042–50. [PubMed: 19679084]
3. Goodey NM, Benkovic SJ. Allosteric regulation and catalysis emerge via a common route. Nat Chem Biol. 2008; 4:474–82. [PubMed: 18641628]

4. Tsai CJ, Del Sol A, Nussinov R. Protein allostery, signal transmission and dynamics: a classification scheme of allosteric mechanisms. Mol Biosyst. 2009; 5:207–16. [PubMed: 19225609]
5. Egerer M, Giesemann T, Herrmann C, Aktories K. Autocatalytic processing of Clostridium difficile toxin B. Binding of inositol hexakisphosphate. J Biol Chem. 2009; 284:3389–95. [PubMed: 19047051]
6. Egerer M, Satchell KJ. Inositol hexakisphosphate-induced autoprocessing of large bacterial protein toxins. PLoS Pathog. 2010; 6:e1000942. [PubMed: 20628577]
7. Reineke J, et al. Autocatalytic cleavage of Clostridium difficile toxin B. Nature. 2007; 446:415–9. [PubMed: 17334356]
8. Shen A. Allosteric regulation of protease activity by small molecules. Mol Biosystems. 2010; 6:1431–1443.
9. Michell RH. Inositol derivatives: evolution and functions. Nat Rev Mol Cell Biol. 2008; 9:151–61. [PubMed: 18216771]
10. Egerer M, Giesemann T, Jank T, Satchell KJ, Aktories K. Auto-catalytic cleavage of Clostridium difficile toxins A and B depends on cysteine protease activity. J Biol Chem. 2007; 282:25314–21. [PubMed: 17591770]
11. Prochazkova K, et al. Structural and molecular mechanism for autoprocessing of MARTX toxin of Vibrio cholerae at multiple sites. J Biol Chem. 2009; 284:26557–68. [PubMed: 19620709]
12. Rupnik M, et al. Characterization of the cleavage site and function of resulting cleavage fragments after limited proteolysis of Clostridium difficile toxin B (TcdB) by host cells. Microbiology. 2005; 151:199–208. [PubMed: 15632438]
13. Shen A, et al. Mechanistic and structural insights into the proteolytic activation of Vibrio cholerae MARTX toxin. Nat Chem Biol. 2009
14. Lupardus PJ, Shen A, Bogyo M, Garcia KC. Small Molecule-Induced Allosteric Activation of the Vibrio cholerae RTX Cysteine Protease Domain. Science. 2008; 322:265–8. [PubMed: 18845756]
15. Pruitt RN, et al. Structure-function analysis of inositol hexakisphosphate-induced autoprocessing in Clostridium difficile toxin A. J Biol Chem. 2009; 284:21934–40. [PubMed: 19553670]
16. Pfeifer G, et al. Cellular uptake of Clostridium difficile toxin B. Translocation of the N-terminal catalytic domain into the cytosol of eukaryotic cells. J Biol Chem. 2003; 278:44535–41. [PubMed: 12941936]
17. Genth H, Dreger SC, Huelsenbeck J, Just I. Clostridium difficile toxins: more than mere inhibitors of Rho proteins. Int J Biochem Cell Biol. 2008; 40:592–7. [PubMed: 18289919]
18. Jank T, Aktories K. Structure and mode of action of clostridial glucosylating toxins: the ABCD model. Trends Microbiol. 2008; 16:222–9. [PubMed: 18394902]
19. Voth DE, Ballard JD. Clostridium difficile toxins: mechanism of action and role in disease. Clin Microbiol Rev. 2005; 18:247–63. [PubMed: 15831824]
20. Kelly CP, LaMont JT. Clostridium difficile--more difficult than ever. N Engl J Med. 2008; 359:1932–40. [PubMed: 18971494]
21. Rupnik M, Wilcox MH, Gerding DN. Clostridium difficile infection: new developments in epidemiology and pathogenesis. Nat Rev Microbiol. 2009; 7:526–36. [PubMed: 19528959]
22. Lyras D, et al. Toxin B is essential for virulence of Clostridium difficile. Nature. 2009; 458:1176–9. [PubMed: 19252482]
23. Aktories K. Self-cutting to kill: new insights into the processing of Clostridium difficile toxins. ACS Chem Biol. 2007; 2:228–30. [PubMed: 17455899]
24. Puri AW, et al. Rational Design of Inhibitors and Activity-Based Probes Targeting Clostridium difficile Virulence Factor TcdB. Chem Biol accepted. 2010
25. Evans MJ, Cravatt BF. Mechanism-based profiling of enzyme families. Chem Rev. 2006; 106:3279–301. [PubMed: 16895328]
26. Greenbaum DC, et al. Small molecule affinity fingerprinting. A tool for enzyme family subclassification, target identification, and inhibitor design. Chem Biol. 2002; 9:1085–94. [PubMed: 12401493]
27. Berger AB, et al. Identification of early intermediates of caspase activation using selective inhibitors and activity-based probes. Mol Cell. 2006; 23:509–21. [PubMed: 16916639]

28. Kato D, et al. Activity-based probes that target diverse cysteine protease families. Nat Chem Biol. 2005; 1:33–8. [PubMed: 16407991]
29. Powers JC, Asgian JL, Ekici OD, James KE. Irreversible inhibitors of serine, cysteine, and threonine proteases. Chem Rev. 2002; 102:4639–750. [PubMed: 12475205]
30. Prochazkova K, Satchell KJ. Structure-function analysis of inositol hexakisphosphate-induced autoprocessing of the Vibrio cholerae multifunctional autoprocessing RTX toxin. J Biol Chem. 2008; 283:23656–64. [PubMed: 18591243]
31. Sheahan KL, Cordero CL, Satchell KJ. Autoprocessing of the Vibrio cholerae RTX toxin by the cysteine protease domain. Embo J. 2007; 26:2552–61. [PubMed: 17464284]
32. Chai J, et al. Crystal structure of a procaspase-7 zymogen: mechanisms of activation and substrate binding. Cell. 2001; 107:399–407. [PubMed: 11701129]
33. Romanowski MJ, Scheer JM, O'Brien T, McDowell RS. Crystal structures of a ligand-free and malonate-bound human caspase-1: implications for the mechanism of substrate binding. Structure. 2004; 12:1361–71. [PubMed: 15296730]
34. Royer CA. Probing protein folding and conformational transitions with fluorescence. Chem Rev. 2006; 106:1769–84. [PubMed: 16683754]
35. Datta D, Scheer JM, Romanowski MJ, Wells JA. An allosteric circuit in caspase-1. J Mol Biol. 2008; 381:1157–67. [PubMed: 18590738]
36. Ferguson AD, et al. Signal transduction pathway of TonB-dependent transporters. Proc Natl Acad Sci U S A. 2007; 104:513–8. [PubMed: 17197416]
37. Suel GM, Lockless SW, Wall MA, Ranganathan R. Evolutionarily conserved networks of residues mediate allosteric communication in proteins. Nat Struct Biol. 2003; 10:59–69. [PubMed: 12483203]
38. Volkman BF, Lipson D, Wemmer DE, Kern D. Two-state allosteric behavior in a single-domain signaling protein. Science. 2001; 291:2429–33. [PubMed: 11264542]
39. Fuentes-Prior P, Salvesen GS. The protein structures that shape caspase activity, specificity, activation and inhibition. Biochem J. 2004; 384:201–32. [PubMed: 15450003]
40. Eisenmesser EZ, et al. Intrinsic dynamics of an enzyme underlies catalysis. Nature. 2005; 438:117–21. [PubMed: 16267559]
41. Fraser JS, et al. Hidden alternative structures of proline isomerase essential for catalysis. Nature. 2009; 462:669–73. [PubMed: 19956261]
42. Lechtenberg BC, Johnson DJ, Freund SM, Huntington JA. NMR resonance assignments of thrombin reveal the conformational and dynamic effects of ligation. Proc Natl Acad Sci U S A. 2010; 107:14087–92. [PubMed: 20660315]
43. Lee GM, Craik CS. Trapping moving targets with small molecules. Science. 2009; 324:213–5. [PubMed: 19359579]
44. Shahian T, et al. Inhibition of a viral enzyme by a small-molecule dimer disruptor. Nat Chem Biol. 2009; 5:640–6. [PubMed: 19633659]
45. Hardy JA, Lam J, Nguyen JT, O'Brien T, Wells JA. Discovery of an allosteric site in the caspases. Proc Natl Acad Sci U S A. 2004; 101:12461–6. [PubMed: 15314233]
46. Scheer JM, Romanowski MJ, Wells JA. A common allosteric site and mechanism in caspases. Proc Natl Acad Sci U S A. 2006; 103:7595–600. [PubMed: 16682620]
47. Pruitt RN, Chambers MG, Ng KK, Ohi MD, Lacy DB. Structural organization of the functional domains of Clostridium difficile toxins A and B. Proc Natl Acad Sci U S A. 2010; 107:13467–72. [PubMed: 20624955]
48. Qa'Dan M, Spyres LM, Ballard JD. pH-induced conformational changes in Clostridium difficile toxin B. Infect Immun. 2000; 68:2470–4. [PubMed: 10768933]
49. Mittal R, Peak-Chew SY, Sade RS, Vallis Y, McMahon HT. The acetyltransferase activity of the bacterial toxin YopJ of Yersinia is activated by eukaryotic host cell inositol hexakisphosphate. J Biol Chem. 2010; 285:19927–34. [PubMed: 20430892]
50. Hanakahi LA, Bartlet-Jones M, Chappell C, Pappin D, West SC. Binding of inositol phosphate to DNA-PK and stimulation of double-strand break repair. Cell. 2000; 102:721–9. [PubMed: 11030616]

51. Macbeth MR, et al. Inositol hexakisphosphate is bound in the ADAR2 core and required for RNA editing. Science. 2005; 309:1534–9. [PubMed: 16141067]

52. Tan X, et al. Mechanism of auxin perception by the TIR1 ubiquitin ligase. Nature. 2007; 446:640–5. [PubMed: 17410169]

53. Leslie AG. Recent changes to the MOSFLM package for processing film and image plate data. Joint CCP4 + ESF-EAMCB Newsletter on Protein Crystallography. 1992; No. 26

54. Potterton E, Briggs P, Turkenburg M, Dodson E. A graphical user interface to the CCP4 program suite. Acta Crystallogr D Biol Crystallogr. 2003; 59:1131–7. [PubMed: 12832755]

55. McCoy AJ, et al. Phaser crystallographic software. J. Appl. Crystallogr. 2007; 40:658–674. [PubMed: 19461840]

56. Adams PD, et al. PHENIX: building new software for automated crystallographic structure determination. Acta Crystallogr D Biol Crystallogr. 2002; 58:1948–54. [PubMed: 12393927]

57. Emsley P, Cowtan K. Coot: model-building tools for molecular graphics. Acta Crystallogr. 2004; D60:2126–32.

58. Davis IW, et al. MolProbity: all-atom contacts and structure validation for proteins and nucleic acids. Nucleic Acids Res. 2007; 35:W375–83. [PubMed: 17452350]

59. DeLano, WL. The PyMOL Molecular Graphics System. DeLano Scientific; San Carlos, CA, USA: 2002.

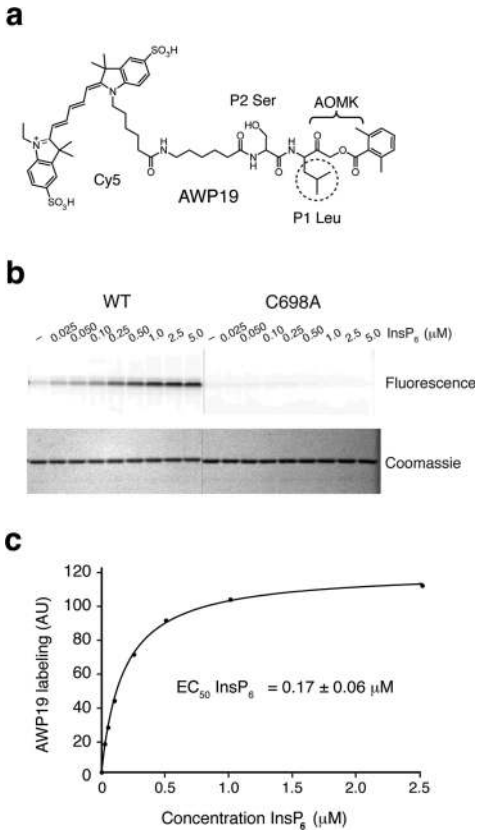

Figure 1.

Development of an activity-based probe assay for measuring TcdB CPD activity. (**a**) Structure of AWP19 activity-based probe. The residues in the peptide specificity element, the acyloxymethyl ketone (AOMK) electrophile, and Cy5 fluorophore are marked. (**b**) $InsP_6$-induced labeling of TcdB CPD by AWP19. Recombinant TcdB CPD was mixed with AWP19 and incubated with the indicated concentration of $InsP_6$. The labeling reactions were resolved by SDS-PAGE, and fluorescence was measured using a flatbed scanner, followed by visualization of total protein using Coomassie staining. No labeling was observed when the catalytic Cys is mutated to Ala. (**c**) Quantitation of EC_{50} (the concentration of $InsP_6$ at which activity is half-maximal) for the AWP19 labeling assay.

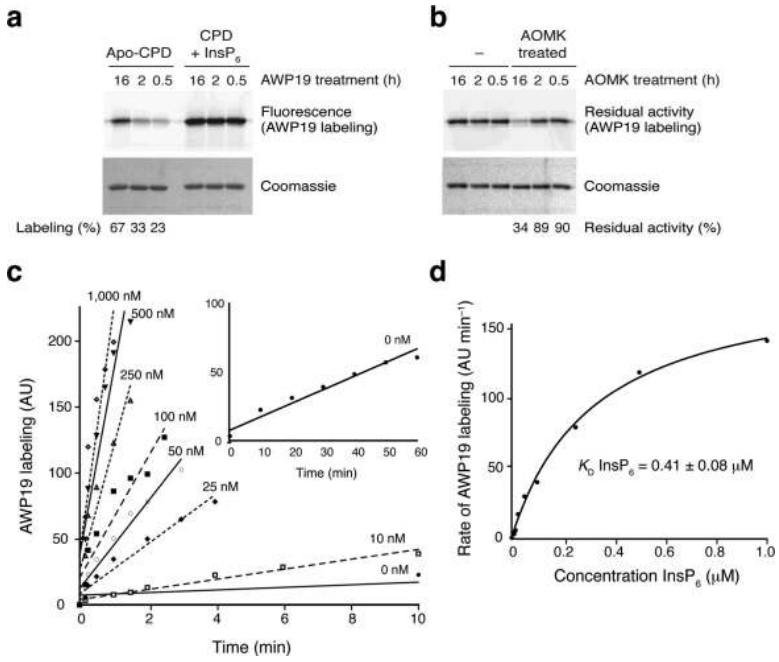

Figure 2.

Detection of an active conformer in the apo-state using an activity-based probe. (**a**) Time-dependent labeling of apo-CPD by AWP19. TcdB CPD, in the absence of exogenous $InsP_6$, was incubated with AWP19 for the indicated period of time, and reactions were resolved by SDS-PAGE. Probe labeling was visualized by fluorescent scanning. The percent labeling was compared relative to TcdB CPD incubated with $InsP_6$ and AWP19 in parallel. (**b**) Pre-incubation of TcdB CPD with an AOMK inhibitor results in time-dependent inhibition of TcdB CPD activity. TcdB CPD was incubated with Ac-GSL-AOMK with or without $InsP_6$ for the indicated times. Residual activity was measured by labeling the enzyme with AWP19 in the presence of $InsP_6$. (**c**) Rate of AWP19 labeling of TcdB CPD in response to increasing $InsP_6$ concentrations. The fluorescent signal (arbitrary units – AU) was plotted against time. (**d**) Rate of AWP19 labeling measured in (c) plotted against $InsP_6$ concentration. AWP19 labeling exhibited Michaelas-Menten like kinetics, allowing for the determination of a dissociation constant of 0.4 μM. This value is in agreement with the published K_D determined using non-enzymatic methods5.

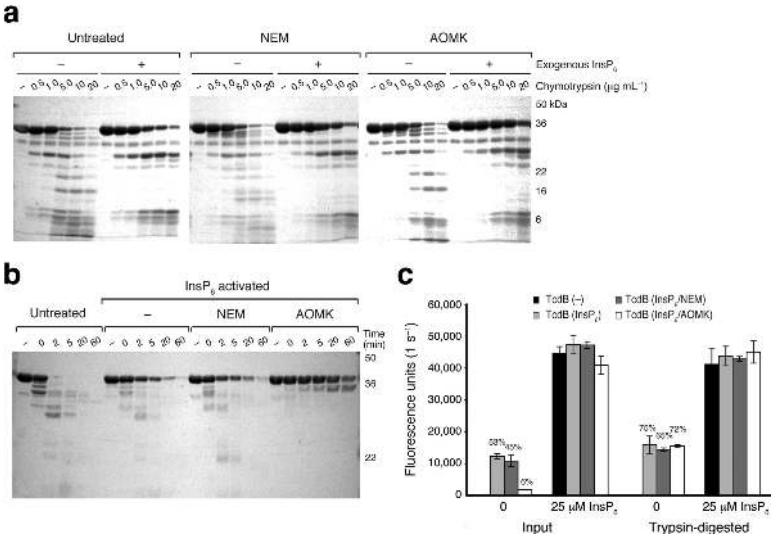

Figure 3.

Effect of $InsP_6$ and P1 Leu inhibitor modification on TcdB CPD conformational mobility. (**a**) Limited proteolysis profile of TcdB CPD variants with and without $InsP_6$. TcdB CPD was either untreated, treated with N-ethylmaleimide (NEM), or treated with Ac-GSLAOMK for 16 hr. TcdB CPD variants were re-purified using the His_6-tag and then subjected to limited proteolysis using chymotrypsin in the absence (–) or presence (+) of $InsP_6$. Reactions were resolved by SDS-PAGE and visualized by Coomassie staining. (**b**) Trypsin digestion of TcdB CPD exposed to $InsP_6$ in the presence or absence of covalent inhibitors. TcdB CPD was activated in the presence of $InsP_6$ alone, or $InsP_6$ and the indicated inhibitor. Treated CPDs were re-purified using gel filtration to remove inhibitor and excess $InsP_6$. Untreated enzyme was also subjected to the same re-purification procedure. Re-purified TcdB CPD variants were digested with trypsin (0.2 mg mL^{-1}), and aliquots were removed at the indicated timepoints and resolved by SDS-PAGE followed by Coomassie staining. (**c**) $InsP_6$ transfer assay. Re-purified TcdB CPD variants from (b) prior to addition of trypsin (input) and after trypsin-digestion (Trypsin) were added to $MARTX_{Vc}$ CPD and fluorogenic substrate cleavage was measured. $InsP_6$ was also added directly to the fluorogenic cleavage assay to determine maximal protease activation of $MARTX_{Vc}$ CPD. The percentages shown above bar graphs indicate the amount of exogenous $InsP_6$ transferred to $MARTX_{Vc}$ CPD relative to the total amount of $InsP_6$ that could have been transferred assuming each TcdB CPD molecule carried a single $InsP_6$ molecule through the re-purification procedure. Values are given as mean ± s.d. (n=3).

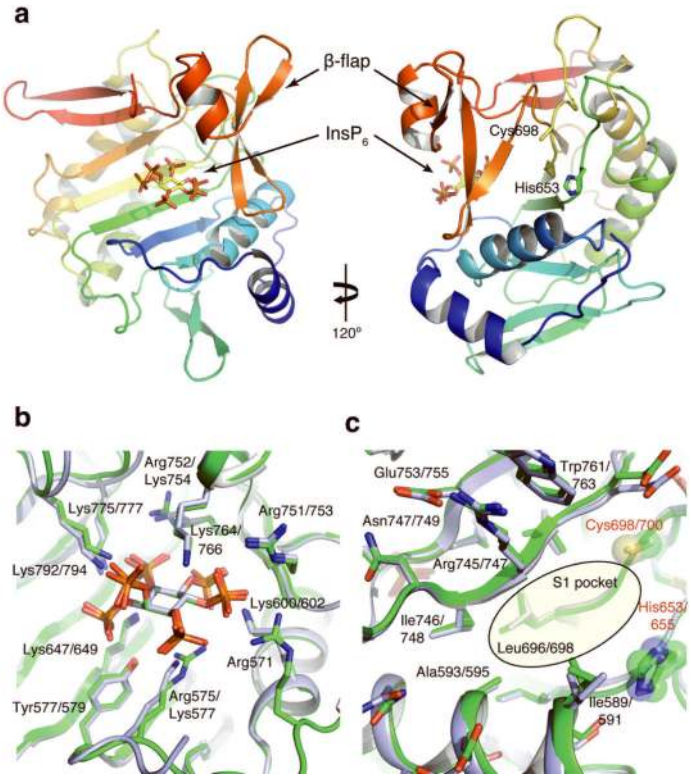

Figure 4.

Structure of TcdB CPD and comparison with TcdA CPD. (**a**) Overview of TcdB CPD structure. The first panel shows the $InsP_6$ binding site, while the second panel shows the structure rotated 120° to reveal the active site. The catalytic Cys and His residues are shown as stick models, and the β-flap and bound $InsP_6$ are labeled. The overall structure is colored from blue at the N-terminus to red at the C-terminus for orientation. (**b**) Overlay of the TcdB (green) and TcdA (light blue) CPD $InsP_6$ binding sites. Sidechains within 3.5 Å of $InsP_6$ are labeled (TcdB/TcdA) and shown as stick models. (**c**) Overlay of the TcdB (green) and TcdA (light blue) CPD active sites. The approximate S1 pocket that interacts with the P1 leucine is shaded. The catalytic Cys and His residues are shown as transparent spheres and labeled in red lettering; conserved residues near the active site are shown as stick models. Residue numbering is given as TcdA/TcdB.

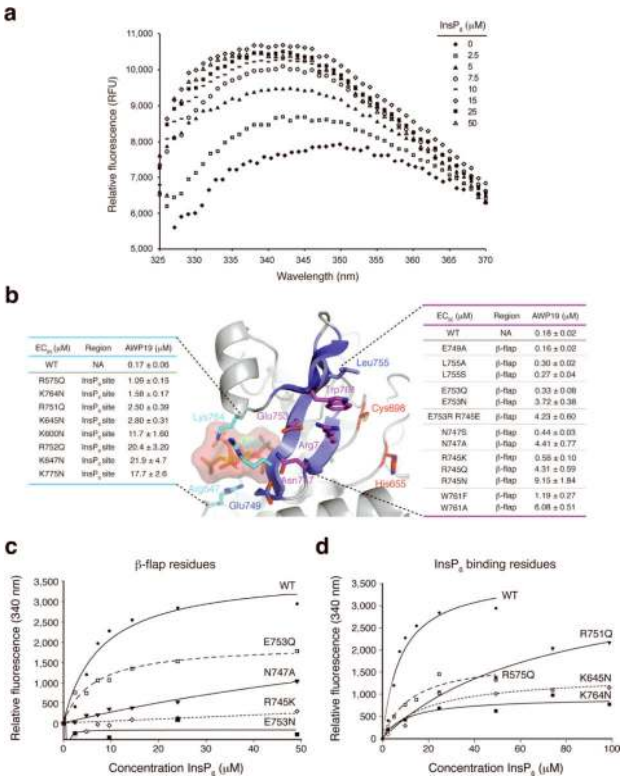

Figure 5.

$InsP_6$ binding induces movement of conserved Trp in β-flap region. (**a**) Effect of $InsP_6$ on intrinsic tryptophan fluorescence of TcdB CPD. TcdB CPD was incubated with the indicated concentration of $InsP_6$, and the fluorescence emission spectra measured after excitation at 295 nm. Fluorescence units (FU) refer to the relative fluorescence $A280^{-1}$. (**b**) Close-up view of β-flap region. The β-flap ribbon structure is colored in purple, and residues required for CPD activity are shown in magenta as sticks. Select $InsP_6$ interacting residues are shown as sticks and colored cyan. Residues dispensable for CPD activity are shown as sticks and colored purple. The EC_{50}s for different point mutants were measured using the probe labeling assay and are expressed as mean ± s.d. (n=3). A lower EC_{50} indicates that the mutant is more sensitive to $InsP_6$. Trp fluorescence emission of (**c**) wild type and β-flap mutants, and (**d**) $InsP_6$ binding mutants at 340 nm was measured in the presence of increasing concentrations of $InsP_6$.

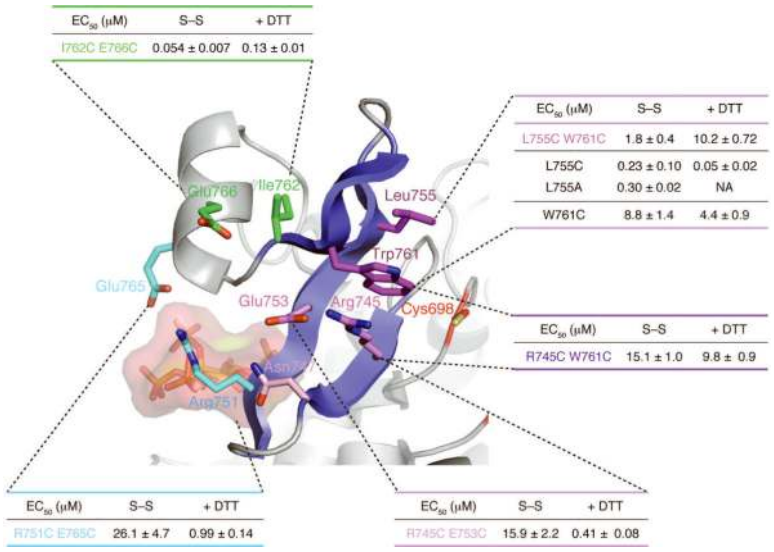

Figure 6.

Effect of redox state on $InsP_6$ responsiveness of engineered disulfide bond mutants in the β-flap. The β-flap is shown as a ribbon structure and colored purple. Residues mutated to Cys as pairs are shown as sticks and colored similarly. Catalytic residues are shown as sticks and colored red. EC_{50} for each mutant is shown in the presence (+DTT) or absence (S-S) of reductant. A lower EC_{50} indicates that the mutant is more sensitive to $InsP_6$. Data are expressed as mean ± s.d. (n=3).

Table 1

Data collection and refinement statistics

	TcdB CPD in complex with $InsP_6$
Data collection	
Space group	C 2
Cell dimensions	
a, *b*, *c* (Å)	128.11, 45.71, 87.35
α, β, γ (°)	90, 103.48, 90
Resolution (Å)	1.0*
R_{merge}	50–2.1 (2.22–2.1)
$I / \sigma I$	8.4 (1.8)
Completeness (%)	97.6 (91.8)
Redundancy	3.2 (2.6)
Refinement	
Resolution (Å)	39.7–2.1
No. reflections	26305/1337
R_{work} / R_{free}	19.2/24.0
No. atoms	
Protein	3854
$InsP_6$	72
Calcium	1
Water	218
B-factors	
Protein	39.2
$InsP_6$	25.6
Calcium	30.1
Water	40.0
R.m.s. deviations	
Bond lengths (Å)	0.008
Bond angles (°)	1.308

*Data was collected from a single crystal. Values in parentheses are for the highest-resolution shell.